Clays and Clay Minerals, Vol. 64, No. 3, 314–333, 2016.

MODELING POWDER X-RAY DIFFRACTION PATTERNS OF THE CLAY MINERALS SOCIETY KAOLINITE STANDARDS: KGA-1, KGA-1b, AND KGa-2

B. A. Sakharov[1], V. A. Drits[1], D. K. McCarty[2]*, and G. M. Walker[2]

[1] Geological Institute, Russian Academy of Sciences, Pyzevskij per. D.7, 109017 Moscow, Russia
[2] Chevron Energy Technology Company (ETC), 3901 Briarpark, Houston, Texas 77042, USA

Abstract—Three kaolinite reference samples identified as KGa-1, KGa-1b, and KGa-2 from the Source Clays Repository of The Clay Mineral Society (CMS) are used widely in diverse fields, but the defect structures have still not been determined with certainty. To solve this problem, powder diffraction patterns of the KGa-1, KGa-1b, and KGa-2 samples were modeled. In a kaolinite layer among three symmetrically independent octahedral sites named as A, B, and C and separated from each other by *b*/3 along the *b* parameter, the A and B sites are occupied by Al cations, whereas, the C sites located along the long diagonal of the oblique kaolinite unit cell are vacant. The layer displacement vectors $\mathbf{t_1}$ and $\mathbf{t_2}$ are related by a pseudo-mirror plane from defect-free 1*T*c kaolinite enantiomorphs, whereas, the random interstratification within individual kaolinite crystallites creates right-hand and left-hand layer sub-sequences producing structural disorder. A third layer displacement vector, $\mathbf{t}_0$, located along the long diagonal of the oblique layer unit cell that contains the vacant octahedral site and coincides with the layer pseudo-mirror plane may exist. Thus, a structural model should be defined by the probability of $\mathbf{t}_1$, $\mathbf{t}_2$, and $\mathbf{t}_0$ layer displacement translations $W\mathbf{t}_1$, $W\mathbf{t}_2$, and $W\mathbf{t}_0$, respectively, determined by simulated experimental X-ray diffraction (XRD) patterns. X-ray diffraction patterns were calculated for structures with a given content of randomly interstratified displacement vectors, and other XRD patterns were calculated for a physical mixture of crystallites having contrasting structural order with only C-vacant layers. The samples differ from each other by the content of high- and low-ordered phases referred to as HOK and LOK. The HOK phase has an almost defect-free structure in which 97% of the layer pairs are related by just the layer displacement vector $\mathbf{t}_1$ and only 3% of the layer pairs form the enantiomorphic fragments. In contrast, the LOK phases in the KGa-1, KGa-1b, and KGa-2 samples differ from HOK phases by the occurrence probabilities for the $\mathbf{t}_1$, $\mathbf{t}_2$, and $\mathbf{t}_0$ layer displacements. In addition, the LOK phases contain stacking faults that displace adjacent layers in arbitrary lengths and directions. Low XRD profile factors (Rp = 8−11%) support the defect structure models. Additional structural defects and previously published models are discussed.

Key Words—Computer simulation, Defect structure, Kaolinite, X-ray diffraction.

INTRODUCTION

Three kaolinite reference samples identified as KGa-1, KGa-1b, and KGa-2 from the Source Clays Repository of The Clay Mineral Society are widely used by clay researchers. These kaolinite samples are representative of commonly occurring, natural kaolinite materials and are distinguished by phase purity and availability. The KGa-1 and KGa-1b samples, often referred to as well ordered or well crystallized kaolinite varieties, were collected from close geographical locations and stratigraphic positions in Georgia (Van Olphen and Fripiat, 1979; Pruett and Webb, 1993; Moll, 2001). The X-ray diffraction (XRD) patterns of KGa-1 and KGa-1b are almost identical and both samples have a similar chemical composition (Pruett and Webb, 1993; Chipera and Bish, 2001; Mermut and Cano, 2001). The KGa-2 standard is also from Georgia (Van Olphen and Fripiat, 1979; Pruett and Webb, 1993; Mermut and Cano, 2001) and has a disordered structure. These kaolinite standards are found in relatively pure deposits, but contain trace quantities of anatase, Fe-oxides, quartz, crandallite, micas, and smectites.

The pure phase composition of KGa-1, KGa-1b, and KGa-2 provides an opportunity for an unambiguous interpretation of experimental data obtained by different methods to investigate the behavior of samples subjected to different treatments and reactions, and to reveal the sensitivity of ordered and disordered kaolinite samples to the same treatments and reactions. For example, these kaolinite standards were used to assign vibration bands in the middle- and near-infrared regions of the infrared (IR) spectra (Madejova and Komadel, 2001; Johnston *et al.*, 1990, 2008; Balan *et al.*, 2001, 2010). Paris (2014) recorded for the first time the ^{27}Al nuclear magnetic resonance (NMR) spectrum of the KGa-1b kaolinite sample at low magnetic field (7T). The analysis of the spectrum allowed determination of the isotropic chemical shift and the quadrupolar interaction parameters. The combination of these data with first principle calculations of the electric field gradient shows that the two adjacent octahedral aluminum sites have different geometry. The KGa-1, KGa-1b, and KGa-2 samples were used to determine kaolinite surface charge proper-

* E-mail address of corresponding author:
dmccarty@chevron.com
DOI: 10.1346/CCMN.2016.0640307

ties (Schroth and Sposito, 1997; Wu, 2001). Investigation of dissolution rates of the KGa-1b and KGa-2 samples in oxalic acid and inorganic acids shows that the fundamental structure of the kaolinites, rather than specific surface details, exerts the greater influence on dissolution kinetics (Sutheimer *et al*., 1999). The KGa-1b and KGa-2 kaolinites were used to study the sorption of uranium (U) to kaolinite from water and more U(VI) was sorbed by KGa-2 than by KGa-1b (Bachmaf and Merkel, 2011). Investigating effects of ultrasound on KGa-1 kaolinite, Franco *et al.* (2004) found that this treatment did not cause amorphization, but introduced stacking faults and formed kaolinite fragments that were enantiomorphic to the main kaolinite matrix.

Different methods and approaches were used to study the transformation of the KGa-1 and KGa-2 kaolinite samples into metakaolinite. Based on the evolution of time-resolved, energy-dispersive powder diffraction patterns of KGa-1 and KGa-2 samples, Bellotto *et al.* (1995) investigated the influence of structural defects on the dehydroxylation reaction. Drits and Derkowski (2015), using the multi-cycle heating and cooling thermogravimetric method, discovered the kinetic behavior of defect-free Keokuk, KGa-1, and KGa-2 samples during partial dehydroxylation. Frost and Vassallo (1996) compared the dehydroxylation reactions of kaolinite KGa-1, dickite, and halloysite using infrared emission spectroscopy and showed that the kaolinite sample lost the inner- and inner-surface hydroxyls simultaneously, whereas, dickite and halloysite lost the inner-surface hydroxyls before inner-hydroxyls.

Recently, the structure of kaolinite has been studied using modern *ab initio* computation methods. White *et al.* (2010), using the density functional theory (DFT) and a step-wise dehydroxylation approach, simulated the local structure of KGa-1b at different stages of partial dehydroxylation. Analysis of the experimental inelastic neutron scattering (INS) spectrum obtained for KGa-1b in combination with DFT analysis were used to determine hydrogen coordinate positions in the kaolinite structure (White *et al.*, 2009, 2013a, 2013b; Sperinck *et al*., 2011). To reconcile the experimental INS data with the DFT analysis, White *et al*. (2013a) concluded that the specific layer displacement vector $\mathbf{t}_0 = -0.3151a - 0.3151b$ is the dominant stacking fault type among other stacking faults present in the KGa-1b structure.

Application of inelastic neutron scattering to analyze the location and dynamics of hydrogen in partially or completely dehydroxylated KGa-1b kaolinite indicated a preferential loss of inner surface H-atoms during partial dehydroxylation, and the residual hydrogen atoms in metakaolinite were located in diverse bonding environments. As with natural KGa-1b kaolinite, the INS spectrum of the partially dehydroxylated sample correlated with the INS spectrum calculated for the defect model containing the specific layer displacement, $\mathbf{t_0}$, and consisting of the contributions from inner- and inner-surface H-atoms (White *et al.*, 2013b).

These mentioned studies are only part of the many publications in which KGa-1, KGa-1b, and KGa-2 were used in diverse scientific, industrial, and other applied fields. A common feature of these and other numerous publications in which these kaolinite samples were used, however, is that the authors do not know the nature of the actual defect structure of the studied kaolinite varieties. For example, the KGa-2 sample is assumed to have structural disorder that is related only to a high proportion of stacking faults (Bookin *et al.*, 1989; Plançon *et al.*, 1989). In contrast, in KGa-1 and KGa-1b, the nature of the structural defects is ambiguous. Stacking faults in the KGa-1 and KGa-1b structure may be distributed either in a mono-phase (Artioli *et al.*, 1995) or in two discrete phases containing contrasting amounts of stacking faults (Plançon *et al.*, 1989).

Because of uncertainties related to the crystal structure of KGa-1b and KGa-2 kaolinite samples, various authors were free to apply models that helped them to interpret their experimental results. Because kaolinite occurs as fine particles, X-ray diffraction is a most convenient and useful technique for crystallographic characterization including stacking disorder. The actual defect structure of kaolinite, however, has apparently not been studied by this method during the last 20 years (Plançon and Tchoubar, 1977; Bookin *et al.*, 1989; Plançon *et al*., 1989, 1990; Artioli *et al*., 1995). During this period, significant progress was achieved in modeling the experimental powder XRD patterns of various highly dispersed and disordered structures of layered minerals (Drits *et al*., 1997a, 2002a,b, 2004, 2011a,b; Ferrage *et al*., 2007; Lanson *et al*., 2009; Lindgreen *et al*., 2002; Plançon *et al*., 1989; Sakharov *et al*., 1999, 2004; McCarty *et al*., 2009). The main task of this paper was to determine the actual defect structure of the CMS kaolinite standards KGa-1, KGa-1b, and KGa-2 by modeling powder XRD patterns.

KAOLINITE DEFECT STRUCTURE (REVIEW)

Kaolinite, $Al_2Si_2O_5(OH)_4$, is a dioctahedral 1:1 layer mineral and the structure consists of one octahedral sheet and one tetrahedral sheet that are bound to each other *via* tetrahedral sheet apical oxygen atoms. Strong cohesion of the adjacent layers is formed by hydrogen bonding from OH groups on the basal surface of one layer to oxygen atoms forming a basal surface of an adjacent layer. The octahedral sheet of the kaolinite layer contains three possible octahedral cation sites differing in the arrangement of OH groups and oxygen atoms, which are labeled A, B, or C (Figure 1) and the 1:1 layers will hereafter be identified and designated by the letter corresponding to the type of vacant site (Bailey, 1963). In the conventional right-hand kaolinite unit cell, the tetrahedral sheet is at the base of each 1:1

https://doi.org/10.1346/CCMN.2016.0640307 Published online by Cambridge University Press

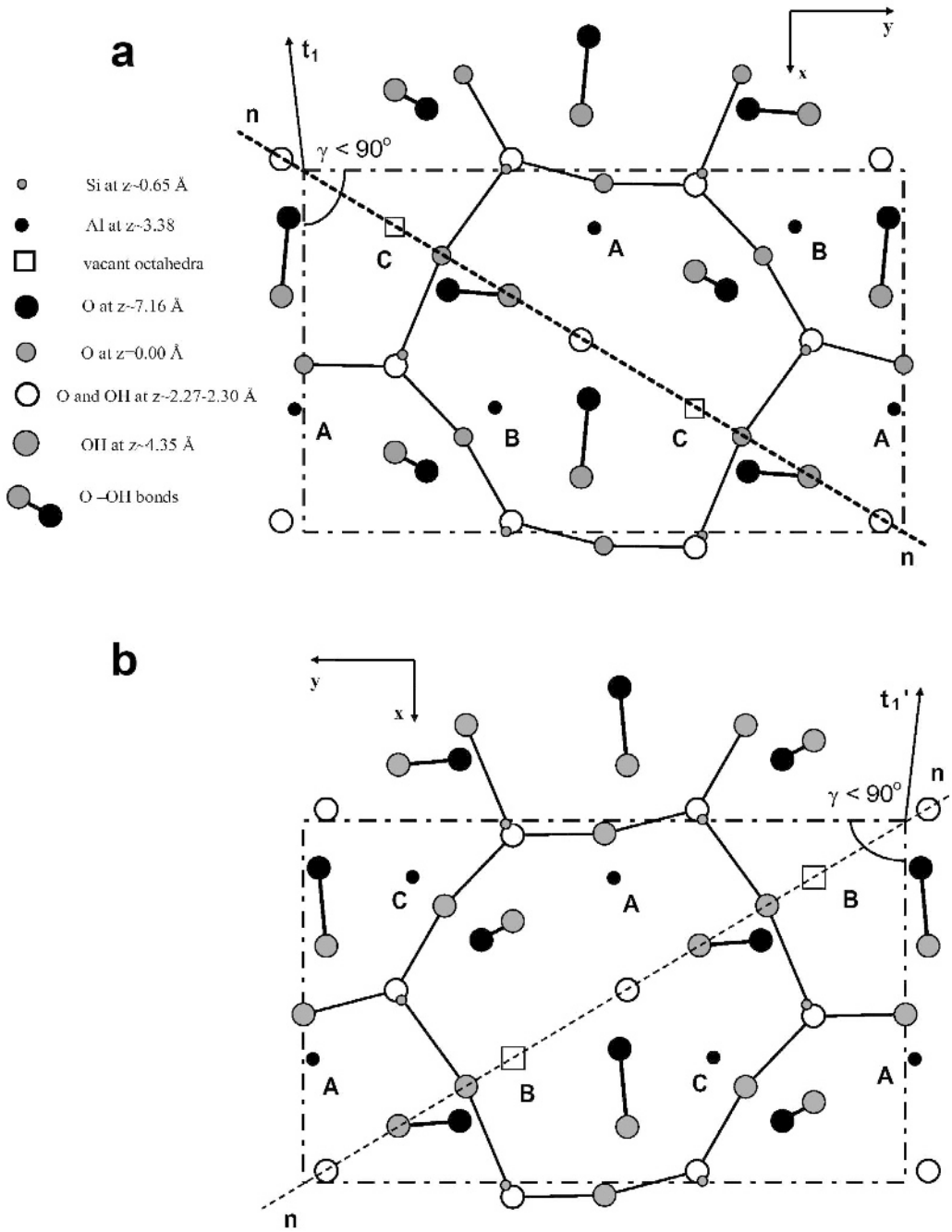

Figure 1. Mutual arrangement of a kaolinite layer; atoms projected on the (001) plane based on the Cartesian atomic coordinates refined by Bish and von Dreele (1989). Possible octahedral sites are labeled A, B, and C. Small black circles indicate octahedral sites occupied by Al, whereas, light squares indicate vacant C sites (a) and vacant B sites (b). Basal oxygen atoms (large black circles) of the upper kaolinite layer paired with basal surface OH groups (small gray circles) of the lower kaolinite layer. The second layer is shifted by $\mathbf{t}_1$ (a) and $\mathbf{t'}_1$ (b) relative to the lower layer. The symbolic notation of kaolinite layer atoms and z-positions are shown (a).

layer and the vacant C site is located along the long diagonal of the unit cell (Bailey, 1963; 1988). Figure 1a shows a fragment of a C vacant layer built using atomic coordinates refined by Bish and von Dreele (1989). A defect-free kaolinite has a one-layer triclinic structure (Brindley and Nakahira, 1958; Bish and von Dreele, 1989).

A characteristic feature of most kaolinite varieties is a defect structure (Brindley *et al*., 1986; Bailey, 1988). The nature of defects in kaolinite structures has been the

https://doi.org/10.1346/CCMN.2016.0640307 Published online by Cambridge University Press

subject of intense discussion for a long time. Bookin *et al*. (1989) carried out a comprehensive analysis of possible defects in the kaolinite structure and concluded that the distortions of a real 1:1 layer structure do not allow stacking faults such as ±120º mutual layer rotations, ±*b*/3 layer translations, and the vacancy displacement model suggested in the literature (Murray, 1954; Brindley and Robinson, 1946; Plançon and Tchoubar, 1977). According to Bookin *et al*. (1989), the two-dimensional layer periodicity of defect-free $1T_C$ kaolinite can be described equally well by the orthogonal cell $\{a_0, b_0, \gamma_0\}$ ($\gamma_0 = 90º$) as well as by the two enantiomorphic oblique cells $\{a_1, b_1, \gamma_1\}$ and $\{a_2, b_2, \gamma_2\}$, which are related to each other by a mirror plane passing through the vacant octahedral site and the center of the ditrigonal ring of the tetrahedral sheet in the kaolinite layer and contains the a_0 axis. The numerical values for the oblique cell coincide with those determined for the defect-free kaolinite sample from Keokuk (Suitch and Young, 1987; Bish and von Dreele, 1989), indicating that the obliquity ($\gamma_{1,2} \neq 90º$) of the refined cell of kaolinite is just the choice of the layer unit cell, and the interlayer stacking sequence does not disturb the layer symmetry.

On the other hand, two oblique layer unit cells and the layer displacement vectors $\mathbf{t}_1$ and $\mathbf{t}_2$, which correspond to individual enantiomorphs and are related to each other by the mirror plane (Figure 2), form the same defect-free 1*T*c kaolinite. A random interstratification of $\mathbf{t}_1$ (approximately $-a_1/3$) and $\mathbf{t}_2$ (approximately $a_1/6-b_1/6$, Figure 2) vectors within individual kaolinite crystallites creates right-hand and left-hand kaolinite structural fragments consisting of the layers with the same vacancy type and, thus, produce most of the structural disorder in kaolinite. Because of the approximately trigonal symmetry of the kaolinite layer, a third layer displacement vector, $\mathbf{t}_0$, located along the mirror plane, may also exist in the kaolinite structure. An accurate model of the defect kaolinite structure should, thus, be defined by the probability of $\mathbf{t}_1$, $\mathbf{t}_2$, and $\mathbf{t}_0$ layer displacement translations $W\mathbf{t}_1$, $W\mathbf{t}_2$, and $W\mathbf{t}_0$, respectively, which can be determined by careful simulation of an experimental XRD pattern. Based on this model, Plançon *et al.* (1989) successfully simulated a set of experimental XRD patterns of natural kaolinite samples and showed that some samples consist of a physical mixture of two distinct populations of kaolinite crystallites, one of which has a low-defect structure and the other a moderate- to high-defect structure. In addition, the model determined by these authors was dominated by C-vacant layers along with a small fraction of B-vacant layers.

Later, Plançon and Zacharie (1990) suggested an alternative approach for the structural characterization of kaolinite based on an expert system which describes the defect structure of kaolinite using a few measurements taken from an experimental powder XRD pattern.

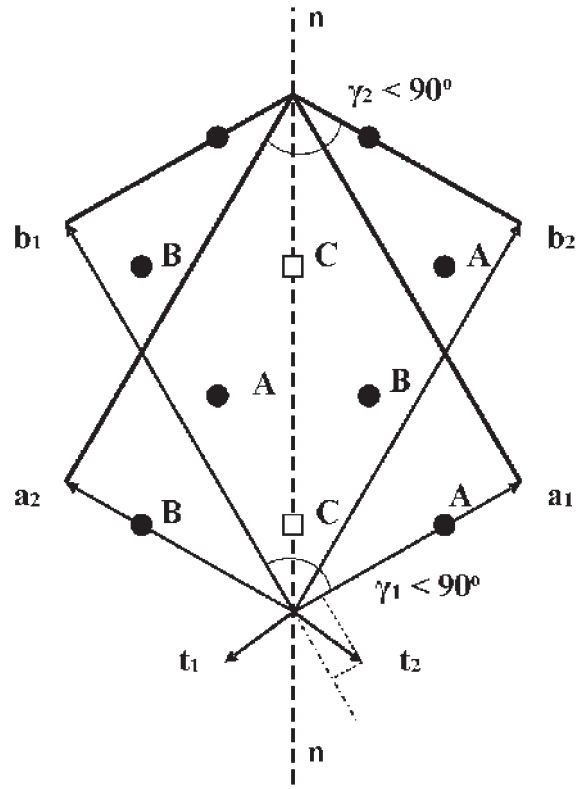

Figure 2. A mutual arrangement of two oblique kaolinite-layer unit cells related by a common pseudo-mirror plane that passes through the centers of vacant C octahedra. The two layer displacements, $\mathbf{t}_1$ and $\mathbf{t}_2$, are related to the corresponding cells by the pseudo-mirror plane.

Application of the expert system to the experimental XRD patterns of nine kaolinite samples whose defect structures were determined by the modeling procedure showed that distinguishing a single phase and quantifying two-phase kaolinite samples is possible.

Interstratification of the right-hand and left-hand structural fragments that consist of the same type of vacant layers in natural kaolinite samples agrees with the results of high-resolution transmission electron microscopy (HRTEM) (Kogure and Inoue, 2005; Kogure *et al*., 2010; Kogure, 2011). These HRTEM studies showed that the common stacking faults in kaolinite are a disorder of the alternative layer displacement vectors, $\mathbf{t}_1$ and $\mathbf{t}_2$. The two layer displacements are related to each other by a pseudo-mirror plane passing through the vacant octahedral site in the kaolinite unit cell. In addition, application of HRTEM revealed the possible existence of stacking faults related to a mutual layer rotation or to displacement of the octahedral vacancy sites.

Artioli *et al*. (1995) proposed a new single-phase model for describing structural disorder in natural kaolinite samples which was based on the stacking of C-vacant and B-vacant layers and the enantiomorphs. According to these authors, the ordered stacking

https://doi.org/10.1346/CCMN.2016.0640307 Published online by Cambridge University Press

sequences of B- and C-enantiomorphic layers represent domains of "monoclinic" kaolinite, like the ordered interstratification of B-layers and C-layers. The four layer types are interstratified and the layer distribution can be described for any total density of stacking faults.

Recently, Ufer *et al*. (2015) applied the Rietveld method for a quantitative phase analysis of kaolinite and pyrophyllite samples. In particular; they showed that the KGa-2 kaolinite sample consists of a single, intermediately disordered phase, whereas, the KGa-1 kaolinite sample is a physical mixture of highly (71.1%) and moderately (28.9%) disordered phases. A similar quantification was carried out for a moderately and a highly disordered pyrophyllite. The potential advantages and limitations of the Rietveld method for mineral quantification of coexisting dioctahedral minerals were also discussed (Ufer *et al*., 2015).

CALCULATION OF POWDER XRD PATTERNS FOR DEFECT STRUCTURAL MODELS OF KAOLINITE

Experimental

Random powder X-ray diffraction patterns from KGa-1 and KGa-2 bulk samples were obtained with a Bruker D8 diffractometer (Bruker AXS, Karlsruhe, Germany (40 kV, 40 mA, Bragg-Bretano mode with a 250 mm goniometer radius) for KGa-1 and KGa-2 and with a Rigaku Smartlab® diffractometer (Rigaku Corporation, Tokyo, Japan) for KGa-1b using CuKα radiation and a graphite crystal monochrometer from 10−65º2θ with a 0.05º2θ step increment and a count time of 100 s/step.

Methodology

One effective approach to obtain quantitative information about the actual defect structure of a fine-grained, dispersed mineral is by modeling the diffraction effects to provide the best agreement between positions, intensities, and profiles of the calculated and observed experimental *hkl* reflections in XRD patterns (Drits and Tchoubar, 1990). To simulate the diffraction effects for kaolinite structural models, the atomic coordinates of the defect-free kaolinite structure refined by Bish and von Dreele (1989) were used with a computer program of Sakharov and Naumov, which is based on algorithms described by Drits and Tchoubar (1990). The main advantages of the program, which was applied for the first time to the study of the kaolinite structure, is that the intensity distribution is calculated for the whole XRD pattern including both 00*l* and *hkl* reflections using the same set of structural parameters. Model structures may contain an arbitrary number of different types of defects and the distribution of the defects may obey an arbitrary value of a short-range order factor. The program can minimize discrepancies between the experimental and calculated XRD patterns.

X-ray diffraction patterns were calculated for kaolinite structural models consisting of a statistically homogeneous population of crystallites, each of which has a given content of the randomly interstratified layer displacement vectors and a set of structural parameters described below. In the calculated models, the crystallites or coherent scattering domains (CSDs) in the *ab* plane have a disk-like shape and different radii, each of which occurs with equal probability. The CSD thicknesses were distributed log-normally along the *c** axis and the parameters of this distribution were determined using the mean thickness of CSDs, equal to the mean number of kaolinite layers, N, multiplied by the layer thickness, and the regression given by Drits *et al*. (1997b). Corrections for instrumental factors, such as horizontal and vertical beam divergence, length, width, and sample thickness were carried out according to the recommendations of Drits *et al*. (1993) and Reynolds (1986). A model of the defect kaolinite structure consisting of the same layer type was defined by the probability of $\mathbf{t}_1$, $\mathbf{t}_2$, and $\mathbf{t}_0$ translations W$\mathbf{t}_1$, W$\mathbf{t}_2$, and W$\mathbf{t}_0$. If the layer displacement vectors are not fixed in length, the variation of the vectors around the average values is described by Gaussian distributions, where δ_x, δ_y, and δ_z are, respectively, the characteristic widths (in fractions of the unit cells) of the distribution along the *a, b*, and *c* directions.

Powder XRD patterns from kaolinite samples may differ because of different mutual orientations of kaolinite particles. The degree of particle orientation was estimated by an angular parameter α equal to the full width at half of a particle distribution (Drits and Tchoubar, 1990). For each particular model, two XRD patterns were calculated using CuKα_1 and CuKα_2 wavelengths and were summed in the ratio of 2:1, respectively. When the structural parameters for each model are fixed, the program automatically seeks the best agreement (minimum R_p factor) between the experimental and calculated XRD patterns by varying the content of each population in a sample. The same program was used to provide a maximum possible agreement between the XRD pattern from a sample consisting of a mixture of two phases named as N and M, respectively, and a XRD pattern simulated as a sum of XRD patterns corresponding to the N and M phases. In this case, the content of N and M phases in the studied sample should be equal to contributions of the XRD patterns of the N and M phases in the XRD pattern of the sample.

Layer displacements used for XRD pattern modeling

Application of the trial-and-error approach showed that the best possible agreements between the experimental and calculated d_{hkl} values can be achieved when the unit cell parameters are: a = 5.1575 Å, b = 8.9474 Å, c = 7.1545 Å, α = β = 90º, and γ = 89.841º and the layer displacement vector $\mathbf{t}_1$ is equal to:

https://doi.org/10.1346/CCMN.2016.0640307 Published online by Cambridge University Press

$$\mathbf{t}_1 = -0.36815\bar{a} - 0.0225\bar{b} + 7.1545\bar{n}$$

where $\bar{n}$ is a unit-cell vector along the c^* axis. This set of the unit-cell parameters differs slightly from that determined by Bish and von Dreele (1989) for the Keokuk sample:

$$a = 5.1554 \text{ Å}, b = 8.9448 \text{ Å}, \gamma = 89.922^\circ,$$
$$\mathbf{t}_1 = -0.36828\bar{a} - 0.0239\bar{b} + 7.1539\bar{n}$$

The second layer displacement vector, $\mathbf{t}_2$, is obtained from $\mathbf{t}_1$ by symmetry to the pseudo-mirror plane of C-vacant layers that passes through the centers of the vacant octahedral sites. As was mentioned, the components of $\mathbf{t}_2$ on the a_1 and b_1 axes are close to $a_1/6$ and $-b_1/6$, respectively (Figure 2). Careful calculations showed that these values are $0.1500a_1$ and $-0.1953b_1$. Taking into account that $a_1 = a$, and $b_1 = b$ and the unit cell is base-centered, the values for the $\mathbf{t}_2$ translation are:

$$\mathbf{t}_2 = -0.3500\bar{a} + 0.3047\bar{b} + 7.1545\bar{n}$$

One can show that the unit-cell parameters determined for the studied samples do not significantly change interatomic distances compared to those obtained using the unit-cell parameters of Bish and von Dreele (1989).

The third layer displacement vector, $\mathbf{t}_0$, is placed along the long diagonal of the unit-cell axis located on the pseudo-mirror plane:

$$\mathbf{t}_0 = -0.3154\bar{a} - 0.3154\bar{b} + 7.1545\bar{n}$$

The modulus of $\mathbf{t}_1$, $\mathbf{t}_2$, and $\mathbf{t}_0$ are equal to each other. Thicknesses of crystallites or coherent scattering domains, CSDs were determined by modeling the profiles of the 001 and 002 reflections. The mean and maximum thicknesses of CSDs having a log-normal distribution are used as variable parameters. Interstratification of $\mathbf{t}_1$ and $\mathbf{t}_2$ layer displacement vectors have a minimal influence on the positions and intensity distribution in the diffraction region containing the triplet of strong maxima having $\bar{1}30$, $\bar{1}\bar{3}1$, and 200 indices. The profiles of these reflections in the experimental XRD patterns were, therefore, initially modeled for the defect-free structure consisting of C-vacant layers. This approach allowed estimation of the radius of the disks in the CSDs and the distribution of discs in the *ab* plane.

SIMULATION OF THE EXPERIMENTAL XRD PATTERNS

KGa-1 sample

Determination of the preliminary estimated parameters allows XRD pattern simulation corresponding to a defect-free model and a model in which layer displacement vectors $\mathbf{t}_1$ and $\mathbf{t}_2$ occur with equal probability and in the same proportion. The comparison of these patterns with that of the KGa-1 sample (Figure 3) indicates at a qualitative level that the sample consists of two phases that differ from each other by the content of stacking faults, where the peak positions of the 02*l* and 11*l* reflections in the experimental XRD pattern and that of the defect-free model almost coincide. This indicates that the highly ordered population of crystallites in the sample named the HOK phase,

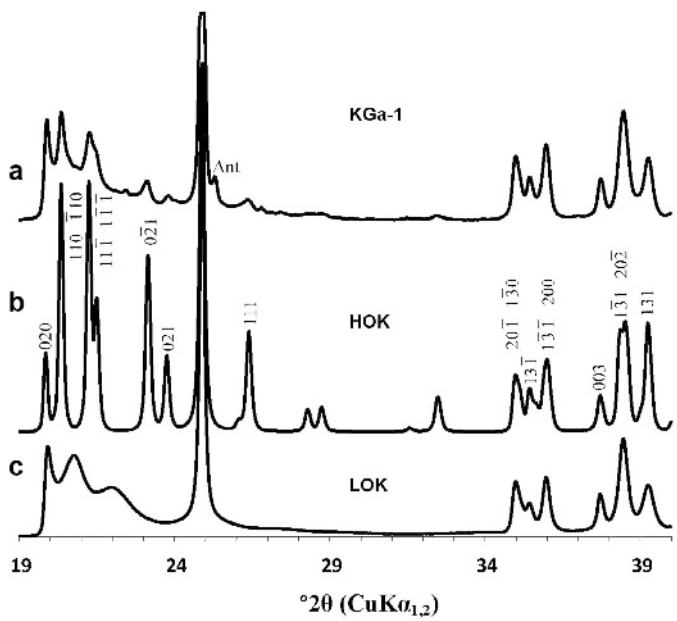

Figure 3. Experimental XRD pattern (a) compared with XRD pattern calculated for the defect-free kaolinite structure (b), and with XRD pattern calculated for the structure with equal amounts of randomly interstratified enantiomorphous kaolinite fragments (c).

https://doi.org/10.1346/CCMN.2016.0640307 Published online by Cambridge University Press

contains only a few stacking faults (Figure 3). The positions of the 11*l* and 02*l* reflections are very sensitive to the relative contents of the layer displacement vector $\mathbf{t}_2$. Calculations showed that an increase of $\mathbf{t}_2$ layer displacements above 5% noticeably shifted the positions of the 02*l* and 11*l* reflections in XRD patterns of the HOK phase relative to those observed in the experimental XRD pattern. The significant background separating individual 02*l* and 11*l* reflections from the base line of the experimental XRD pattern probably are due to the contribution of a low ordered population of crystallites named the LOK phase.

The defect structure of each of the coexisting phases in the sample was determined by a trial and error method by variation in defect types, defect occurrence, and the content of the phases. The maximum possible agreement between the experimental and modeled powder XRD patterns of the KGa-1 sample was achieved using a set of parameters that described the defect structural models of the HOK and LOK phases (Table 1). The HOK phase has an almost defect-free structure in which 97% of the layer pairs are related by the layer displacement vector $\mathbf{t}_1$ and only 3% of the layer pairs form enantiomorphic fragments. In contrast, the LOK phase has three $\mathbf{t}_1$, $\mathbf{t}_2$, and $\mathbf{t}_0$ layer displacements that occur in ratios 0.55:0.35:0.05 and are interstratified at random.

Two distinct features exist between the HOK and LOK the phases. First, the LOK phase contains 5% stacking faults due to layer displacement by $\mathbf{t}_0$. This kind of defect slightly improves the quality of the agreement between the experimental and calculated XRD patterns. Model calculations show, even visually, that the agreement between the experimental and calculated XRD patterns is worse when the LOK phase has no stacking faults from $\mathbf{t}_0$ layer displacements (not shown). The second difference between the probability parameters describing the coexisting phases is the presence of 5% of arbitrary stacking faults, W_a, in the LOK phase which displace adjacent layers with respect to each other in arbitrary directions and lengths (details in Drits and Tchoubar, 1990).

The XRD patterns corresponding to the HOK and LOK crystallite populations (Figure 4) taken in proportion 24.3% and 75.7%, respectively, provides the optimal agreement between the experimental and calculated XRD patterns at Rp = 8.12%. This result shows that the sample consists of a physical mixture of 24.3% HOK and 75.7% LOK phases. The proportion of the LOK to HOK phase determined in this work is close to that of similar phases in the KGa-1 sample (29:71) quantified by the Rietveld method (Ufer *et al*., 2015). Three fragments of the experimental XRD pattern and patterns of the HOK and LOK phases presented in a larger scale shows that the HOK crystallites contribute significantly to the positions, widths, and intensities of the 02*l* and 11*l* reflections, whereas the LOK crystallites

Table 1. Structural parameters of HOK and LOK fractions in KGa-1, KGa-1b, and KGa-2.

Unit cell parameters of kaolinite phase	*a* (Å)	*b* (Å)	*c** (Å)	γ (deg)	$\mathbf{t}_1$	$\mathbf{t}_2$	$\mathbf{t}_0$
HOK	5.1575	8.9474	7.1545	90	$-0.3681a - 0.0225b$	$-0.3499a + 0.3047b$	$-0.3154a - 0.3154b$
LOK	5.1575	8.9474	7.1545	90	$-0.3681a - 0.0225b$	$-0.3499a + 0.3047b$	$-0.3154a - 0.3154b$

Sample	KGa-1		KGa-1b		KGa-2_1	
Phase	HOK	LOK	HOK	LOK	HOK	LOK
W($\mathbf{t}_1$)	0.97	0.55	0.97	0.55	0.97	0.55
W($\mathbf{t}_2$)	0.03	0.35	0.03	0.38	0.03	0.35
W($\mathbf{t}_0$)	–	0.05	–	0.05	–	0.05
Wa	–	0.05	–	0.02	–	0.05
δ(**t**)	0.05*c*	0.02*a*, 0.02*b*, 0.05*c*	0.05*c*	0.02*a*, 0.02*b*, 0.05*c*	0.03*a*, 0.02*b*, 0.05*c*	0.02*a*, 0.02*b*, 0.05*c*
N	45	45	45	45	25	25
D (Å)	200–800	200–800	200–800	200–800	200–800	200–500
α (deg)	80	80	180	180	150	150
C (%)	24.3	75.7	28.4	71.6	4.0	96.0

Wa is the amount of arbitrary stacking faults which displace adjacent layers with respect to each other in arbitrary directions and lengths (see details in Drits and Tchoubar, 1990), *N* is the mean number of layers in coherent scattering domain (CSD), *D* (Å) is CSD diameter, α is a factor estimating the degree of particle orientation.

https://doi.org/10.1346/CCMN.2016.0640307 Published online by Cambridge University Press

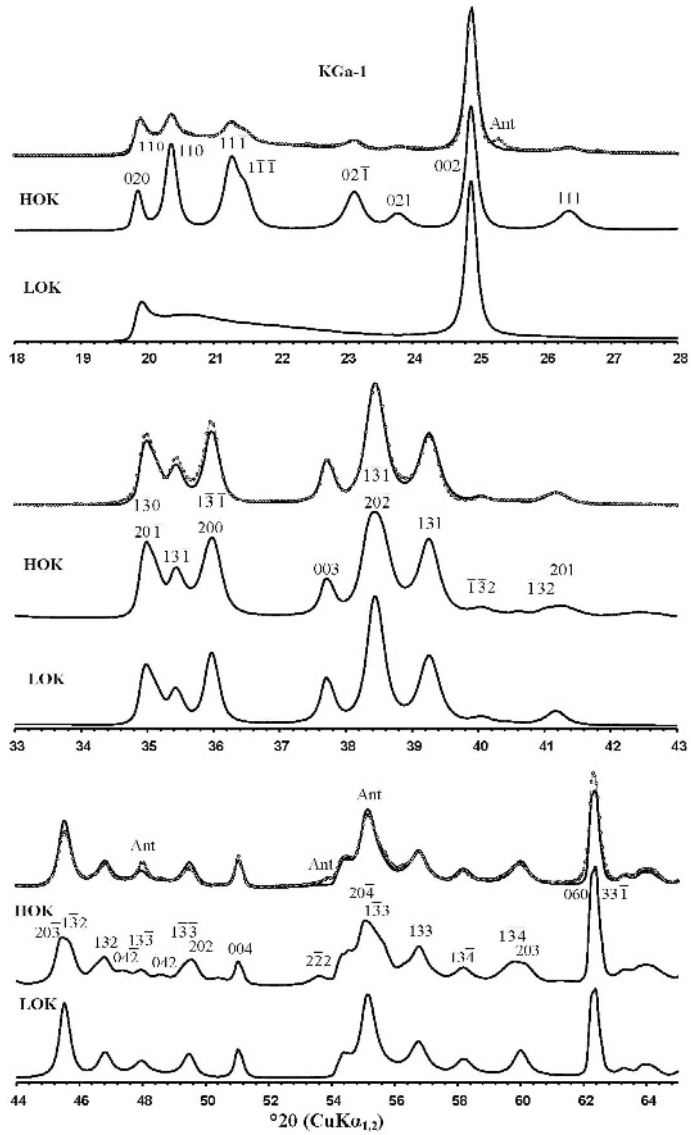

Figure 4. Most diagnostic parts of experimental KGa-1 XRD pattern (dotted line) showing agreement with patterns obtained by optimal summation of the calculated XRD patterns (solid line) of the HOK and LOK components.

contribute to the background in a non-uniform manner along with the profile of the 020 reflection (Figure 4).

KGa-1b sample

Modeling of the experimental XRD pattern of the KGa-1b sample showed that the phase composition of the sample is similar to that of KGa-1. Both samples consist of HOK and LOK phases, and both have the same unit cell parameters and identical sets of probability parameters (Table 1). The HOK phases in both samples have the same ratios of the $\mathbf{t}_1$ and $\mathbf{t}_2$ layer displacements, whereas, in the LOK phase, the relative contents of layer displacements $\mathbf{t}_2$, $\mathbf{t}_0$, and arbitrary stacking faults are equal to 0.38, 0.05, and 0.02 instead of 0.35, 0.05, and 0.05 determined for the LOK of the KGa-1 sample (Table 1). The XRD patterns corresponding to the HOK and LOK crystallite populations (Figure 5) taken in proportions of 28.4% and 71.6%, respectively, provided the optimal agreement between the experimental and calculated patterns at Rp = 9.74%. The main difference between the KGa-1b and KGa-1 samples is, thus, that KGa-1b contains a higher content of the HOK phase (28.4%) compared with KGa-1 (24.3%).

KGa-2 sample

The best possible agreement between the experimental and modeled powder XRD patterns (Figure 6) was based on a set of probability parameters that described the defect structural model of the HOK and LOK phases (Table 1) from modelling the whole XRD pattern. The

https://doi.org/10.1346/CCMN.2016.0640307 Published online by Cambridge University Press

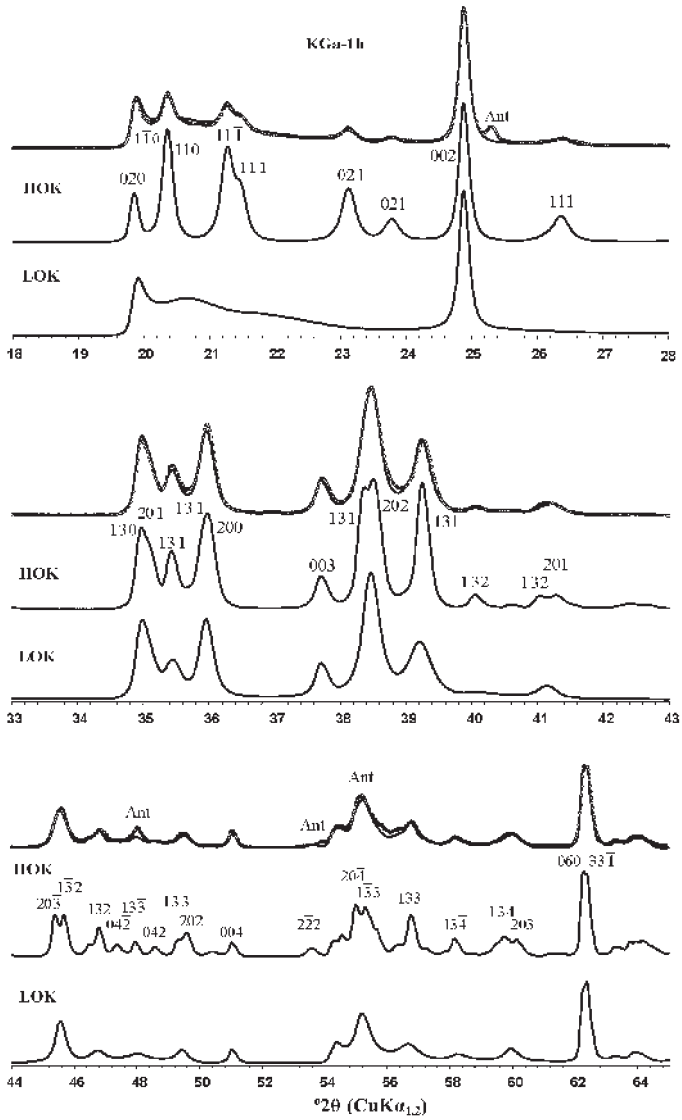

Figure 5. Most diagnostic parts of an experimental KGa-1b XRD pattern (dotted line) showing agreement with patterns obtained by optimal summation of the calculated XRD patterns (solid line) of the HOK and LOK components.

results of the modeling show that the KGa-2 sample also consists of two populations of crystallites with the same unit cell parameters as those found for the HOK and LOK phases of KGa-1 and KGa-1b. In one of the populations, crystallites have an almost defect-free structure identical to that determined for the KGa-1 and KGa-1b samples. In this phase, 97% of the layer pairs are related by the layer displacement vector $\mathbf{t}_1$ and 3% of the layer pairs form enantiomorphic fragments. As in the LOK phases of KGa-1 and KGa-1b, this phase along with the high amount of $\mathbf{t}_1$ (55%) and $\mathbf{t}_2$ (35%) interlayer displacements contains 5% of the layer displacement $\mathbf{t}_0$ and 5% of arbitrary stacking faults (Table 1). The best agreement between the model and experimental XRD patterns was achieved with the HOK and LOK phases in the proportion 0.96:0.04 with Rp = 10.8% (Figure 6).

Results obtained by expert system of Plançon and Zacharie (1990)

Application of the expert system to the XRD patterns of the KGa-1, KGa-1b, and KGa-2 samples showed that a monophase defect structure of KGa-2 can be distinguished from a two-phase structure of KGa-1 and KGa-1b. The expert system and modeling results from this study showed that the kaolinite samples consist of only C-vacant layers. In addition, for the KGa-1 and KGa-1b samples, the proportion of the HOK and LOK phases determined by XRD modeling (24.4:75.6; 28.4:71.6) differed significantly from the ratios found by the expert system (34.3:65.7; 39.9:60.1).

https://doi.org/10.1346/CCMN.2016.0640307 Published online by Cambridge University Press

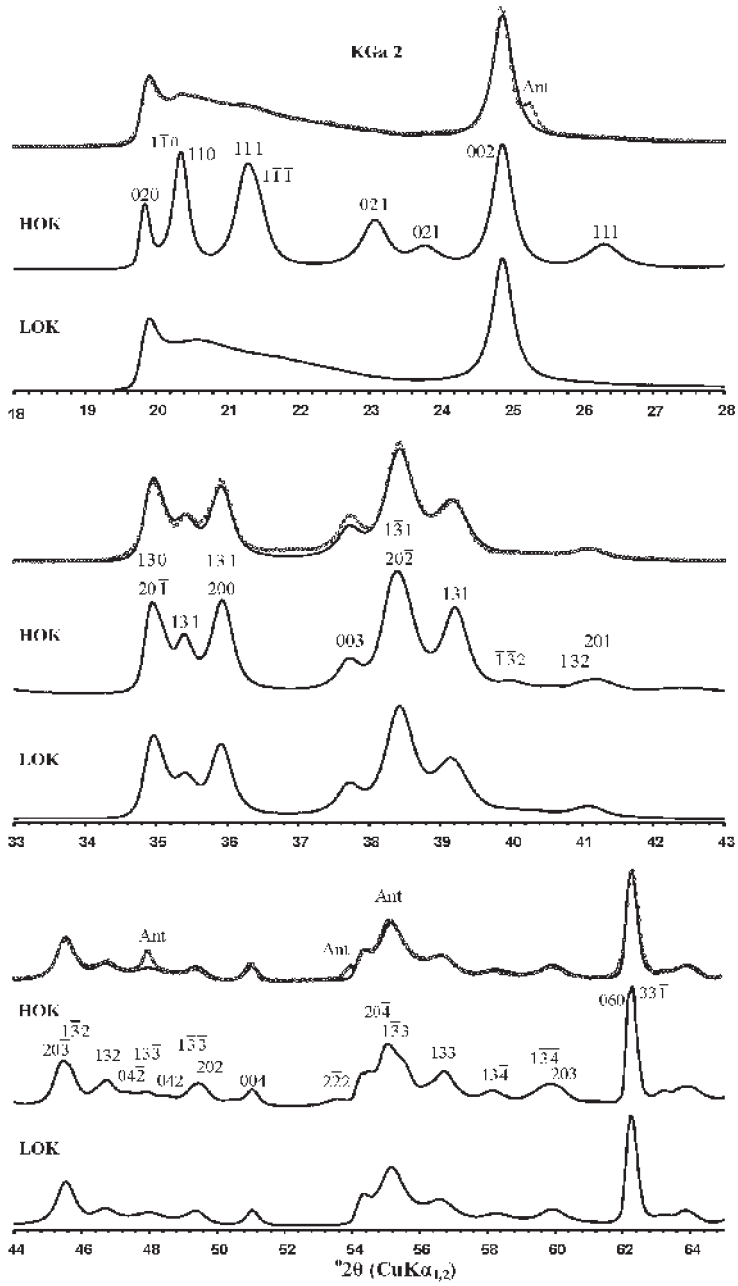

Figure 6. Most diagnostic parts of an experimental KGa-2 XRD pattern (dotted line) showing agreement with patterns obtained by optimal summation of the calculated XRD patterns (solid line) of the HOK and LOK components.

The expert system cannot provide information about structural disorder of the LOK phases in these samples and will not separately distinguish $\mathbf{t}_2$ and $\mathbf{t}_0$ layer displacements. The system will, therefore, give only a global abundance of translation defects, p, equal to the ratio known as the Hinckley Index, HI (Hinckley, 1963; Plançon and Zacharie, 1990). The HI value determined for KGa-2 was 0.22, whereas, the sum of $W\mathbf{t}_2 + W\mathbf{t}_0$ determined by the XRD modelling of this sample was 0.40 (Table 1).

DISCUSSION

The main aim of this work was to determine types of defects and patterns of distribution in the kaolinite structures of the KGa-1, KGa-1b, and KGa-2 samples. The good agreement between the experimental and calculated XRD patterns obtained for the whole 10–65°2θ diffraction range with low profile fitting factors (Rp = 8–11%) is strong evidence for the validity of the defined defect models (Figure 7). These samples consist of only C-vacant layers and the main source of

https://doi.org/10.1346/CCMN.2016.0640307 Published online by Cambridge University Press

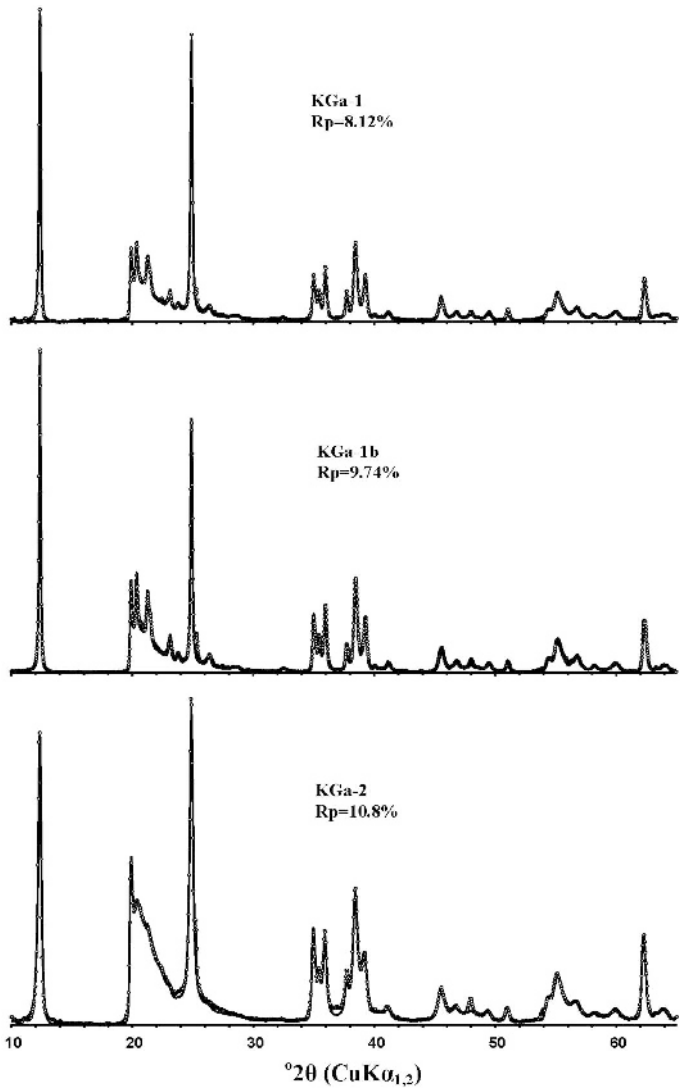

Figure 7. Comparison of the experimental and simulated XRD patterns of KGa-1, KGa-1b, and KGa-2.

defects in the structures is random interstratification of enantiomorphic kaolinite fragments related to each other by a pseudo-mirror plane and due mostly to the layer displacement vectors $\mathbf{t}_1$ and $\mathbf{t}_2$.

The samples contain two populations of crystallites with different contents of stacking faults and were distinguished from each other by the relative amounts of the HOK and LOK phases. Surprisingly, in the so-called well ordered or well crystallized KGa-1 and KGa-1b kaolinites, the relative amounts of the HOK phases were equal only to 24.3 and 28.4%, which are, respectively, 3 and 2.5 times lower than the coexisting LOK phases. Comparison of the XRD patterns of the HOK and LOK phases that compose KGa-1,KGa-1b, and KGa-2 showed that the positions and general shape of the intensity distribution in XRD patterns of the LOK phases were almost identical, which means that KGa-1 and KGa-1b differ from KGa-2 mostly by the higher content of the HOK phase. The coexistence of HOK and LOK phases in natural kaolinite samples discovered by Plançon *et al.* (1989) is, thus, in full agreement with the results of the present study.

Models for the stacking faults in kaolinite

Defects in crystallites characterized by one layer type. The symmetrical arrangement of atoms with respect to the pseudo-mirror plane (Figure 1a) suggests a most favorable model for stacking faults. Indeed, assume that the displacement of a layer with respect to the preceding one is described by $\mathbf{t}_1$. If a regular crystal is formed, all successive layers are shifted by the same vector $\mathbf{t}_1$. A layer that is related to the previous one by the pseudo-mirror plane, *n*, creates a stacking fault and the plane acts as a glide plane for these two layers, while both the

https://doi.org/10.1346/CCMN.2016.0640307 Published online by Cambridge University Press

periodicity and the cation distribution would remain unchanged. The formation of such a layer would, therefore, lead to only minor changes in the potential energy of layer interaction, as well as in the hydrogen bond energy. The $\mathbf{t}_2$ vector, which is related to $\mathbf{t}_1$ by the same *n* plane, would be the new translation for a crystal fragment between the "defect" layer and the next stacking fault. The second defect-free fragment thus formed should be enantiomorphic to the first one. Because in the kaolinite layer n and m planes almost coincide (Figure 2), a pair of layers related by the glide plane should coincide with each other. The model of interstratification of enantiomorphic layers, thus, becomes that of alternating identical layers stacked with symmetrical translations $\mathbf{t}_1$ and $\mathbf{t}_2$. The results of the present work as well as those obtained by modeling of the XRD patterns (Plançon *et al.*, 1989) and HRTEM (Kogure and Inoue, 2005; Kogure *et al*., 2010, 2011) show that, among the different types of stacking faults, those corresponding to $\mathbf{t}_1$ and $\mathbf{t}_2$ layer interstratification displacements are most abundant. Bookin *et al*. (1989) considered two extreme modes of occurrence of $\mathbf{t}_1$ and $\mathbf{t}_2$ vectors in the defective kaolinite structure consisting of C-vacant layers. The first mode includes interstratification of the enantiomorphic packets each of which has an ordered layer stacking, whereas, in the second mode isolated $\mathbf{t}_2$ stacking faults are inserted occasionally in the ordered matrix with $\mathbf{t}_1$.

The first mode was first visualized by application of HRTEM to a diagenetic kaolinite sample with images that demonstrated two types of ordered packets having $\mathbf{t}_1$ and $\mathbf{t}_2$ layer translations (Kogure and Inoue, 2005). A similar pattern in the distribution of stacking faults exists in the defect structures of KGa-2 and the LOK phases of KGa-1 and KGa-1b (present work). Indeed, in these structures stacking faults result from the disorder in alternating $\mathbf{t}_1$, $\mathbf{t}_2$, and $\mathbf{t}_0$ layer displacements among which $\mathbf{t}_1$ and $\mathbf{t}_2$ occur in commensurable proportions (Figure 8a). This type of stacking fault distribution in the defect kaolinite structure has been called a "growth fault" (Bookin *et al*., 1989) and "enantiometric twins" (Kogure and Inoue, 2005).

The second type of stacking fault distribution in the defect kaolinite structure was observed by HRTEM in a kaolinite specimen of sedimentary origin (Kogure *et al*., 2010). In this case, thick periodic packets with $\mathbf{t}_1$ (or $\mathbf{t}_2$) were seldom separated from each other by isolated stacking faults with $\mathbf{t}_2$ or ($\mathbf{t}_1$). The HOK phase calculated for KGa-1 and KGa-1b has this mode of stacking faults. Indeed, interstratification of 3% layer pairs with $\mathbf{t}_2$ and 97% layer pairs with $\mathbf{t}_1$ should provide a defect structural model of the HOK structure in which the layer sequence related by $\mathbf{t}_1$ was seldom interrupted by a single layer with $\mathbf{t}_2$ (Figure 8b).

Stacking disorder by layer rotation and/or displacement of vacant octahedral sites. Application of HRTEM to the kaolinite sample of sedimentary origin previously studied by Johnston *et al*. (2008) showed that along with interstratification of left- and right-hand structural fragments, the studied kaolinite sample contains another type of stacking disorder related to either mutual layer rotation or to displacement of the vacant octahedral site in the kaolinite layer (Kogure *et al*., 2010; Kogure, 2011). The geometrical analysis of these stacking faults carried out by Bookin *et al*. (1989) showed that the sequence of kaolinite layers containing stacking faults formed due to layer rotation and the octahedral vacancy displacements cannot be described in terms of the same lattice without mutual layer distortion. This distortion probably increases the energy of the formation of these stacking faults, thus decreasing the occurrence probability.

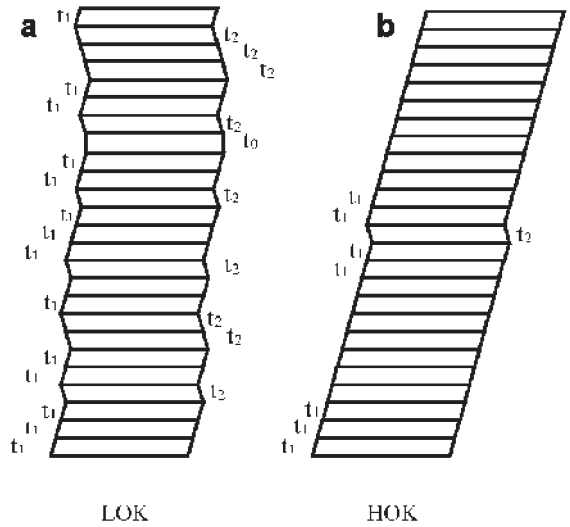

Figure 8. Schematic illustration of two types of structural disorder in KGa-1, KGa-1b, and KGa-2. One type of disorder is from random interstratification of thin enantiomorphic blocks (a) and is similar to KGa-2 and LOK phase structures in which layer displacements $\mathbf{t}_1$ and $\mathbf{t}_2$ occur in compatible proportions (Table 1). The second type of disorder corresponds to the HOK phase because structural periodicity is seldom disturbed by isolated stacking faults (b).

Potential possibility of additional defects in kaolinite structures

Occurence of B-vacant layers. The possible coexistence of C- and B-vacant layers in a kaolinite structure should be accompanied by some crystal-chemical restrictions that create the specific features in an XRD pattern. The regular interstratification of C- and B-vacant layers forms the dickite structure in which both layer types have the same displacements along the *a* axis as that in an idealized 'monoclinic' kaolinite structure (Bailey, 1963,1988). A structural comparison of C-vacant and B-vacant kaolinite layers (Figure 1a,b) shows that the layers are different because the pseudo-mirror planes are

https://doi.org/10.1346/CCMN.2016.0640307 Published online by Cambridge University Press

rotated with respect to each other by ~120º, and the *a* and *b* parameters of the unit cells form the acute angle ($\gamma < 90º$) located at the opposite ends of the *b* parameter common for both cells. In contrast, the *a* parameter of the cells are slightly inclined toward each other to form the same acute angle γ. The octahedral vacancy in regular kaolinite is, therefore, always near the acute angle γ.

In the dickite structure, because of the ordered interstratification of C- and B-vacant layers, the lateral sizes of layers adjust to each other owing to the transformation of the interstratified oblique unit cells with $\gamma > 90º$ and $\gamma < 90º$ to the common orthogonal layer cell with $\gamma = 90º$. In contrast, irregular interstratification of the layer types having comparable contents should be accompanied by strain from a mutual deformation of the layer lattice periodicities in the BC and CB layer pairs. Due to the minor variation of γ from 90º, however, a small amount of B-vacant layer imperfections may occur in the C-layer matrix. These C layers may also introduce some strain, but the influence on diffraction effects should be negligible.

In order to visualize diffraction effects in coexisting C and B layers, the layer displacements related to different types of the layer pairs must be defined. As was mentioned, the acute angle $\gamma < 90º$ in C-vacant and B-vacant layers should be formed at opposite ends of the *b* parameter of the unit cells providing incommensurable stacking of CB and BC layer pairs. For a given choice of *z* direction from tetrahedral to octahedral sheets, the interlayer shift is defined unambiguously by the vacant site in the preceding layer. Indeed, the positions of the basal oxygen atoms of the growing upper layer are predetermined by the positions of OH groups forming the upper basal surface of the lower preceding layer and controlling formation of the most stable interlayer hydrogen bonds. The positions of surface OH groups of the preceding layer are, therefore, predetermined positions of the tetrahedral sheet of the upper layer independent of the positions of vacant octahedral sites in this layer (Figure 1a,b). Thus, the transition from C to B or C layer in the sequence CB or CC is determined by the layer displacement vector $\mathbf{t}_1$. In contrast, to carry out the transition from B to C or B layer in the sequence BC or BB layer pairs, the layer displacement vector should have the opposite sign along the y-component, which is:

$$(\mathbf{t}_1)_{BC} = (\mathbf{t}_1)_{BB} = -0.36815\bar{a} + 0.0225\bar{b} + 7.1545\bar{n}$$

Comparison of the experimental XRD patterns of the KGa-1 and KGa-2 samples with those of their two-phase models in which the LOK phases contain 10% B-vacant layers shows that the main diffraction effect of B layers is the shift of the 131 reflection to the nearest $1\bar{3}1$ reflection toward a lower 2θ angle along with decreasing resolution (Figure 9b,d). This effect is most clearly seen in the comparison of the experimental and calculated patterns of KGa-2, and is not obvious in the XRD pattern of KGa-1. In order to reveal a small amount of B-layers (<5%) in kaolinite samples with XRD patterns similar to KGa-1, experimental XRD patterns must have high statistics, careful calibration, and accurate instrumental correction factors. Even in this case, the reliable determination of a small amount of B-vacant layers may be ambiguous because similar diffraction effects may be created from layer displacements by $\mathbf{t}_0$. Plançon *et al*. (1989), however, determined a coexisting small amount of B layers among C layers and Kogure *et al*. (2010) admitted the existence of local dickite-like fragments formed by layer subsequences C-B-C in a particular kaolinite sample of sedimentary origin which had an IR spectrum that contained dickite bands (Johnston *et al*., 2008).

Layer displacements by $\mathbf{t}_1 - b/3$. Among the possible stacking faults in kaolinite structures are effects that originate due to the layer displacement vector $\mathbf{t}_1 - b/3$ (Table 1). Brindley (1980) suggested these types of stacking faults by assuming that such displacement does not disturb the mutual arrangement of basal oxygen and hydroxyls of adjacent layers. In the case of the interlayer shift by $-b/3$, however, the octahedral cations of the lower layer should be located exactly under the tetrahedral Si atoms of the upper layers. As noted by Newnham (1961) and supported by the electrostatic energy calculations of Giese (1982), this arrangement is energetically unfavorable. The origin of the $\mathbf{t}_1 - b/3$ layer displacement, however, is possibly related to post-crystallization mechanical effects (Bookin *et al*., 1989).

Comparison of the experimental XRD patterns obtained in this study with those calculated for structural models in which the LOK phases contain 10% of the $\mathbf{t}_1 - b/3$ layer displacements shows that at this stage of modeling, this amount of these stacking faults contributes selectively to the different parts of the XRD patterns. Indeed, the mutual displacement of the adjusted layer by $b/3$ along the *b* axes does not influence the positions and intensities of 20*l* and 13*l* reflections (not shown). In contrast, this type of stacking fault disturbs the positions and intensities of 02*l* and 11*l* reflections (Figure 10). In general, a model containing a small amount of B-vacant layers, $\mathbf{t}_1$-$b/3$ stacking faults, or

Figure 9 (*facing page*). Parts of experimental KGa-1 XRD patterns showing agreement with reflections in the 02*l*, 11*l* (a) and 20*l*, 13*l* (b) regions for patterns obtained by the optimal summation of calculated HOK and LOK components, where LOK contains 10% B-vacant layers. Parts of the experimental KGa-2 XRD patterns showing agreement with reflections in the 02*l*, 11*l* (c) and 20*l*, 13*l* (d) regions for patterns obtained by the optimal summation of calculated HOK and LOK components, where LOK contains 10% B-vacant layers.

https://doi.org/10.1346/CCMN.2016.0640307 Published online by Cambridge University Press

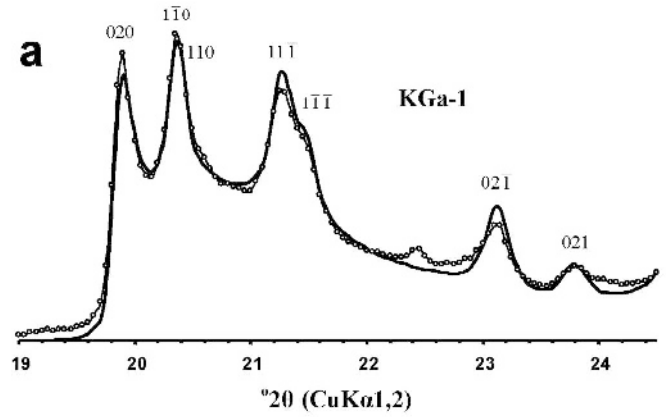

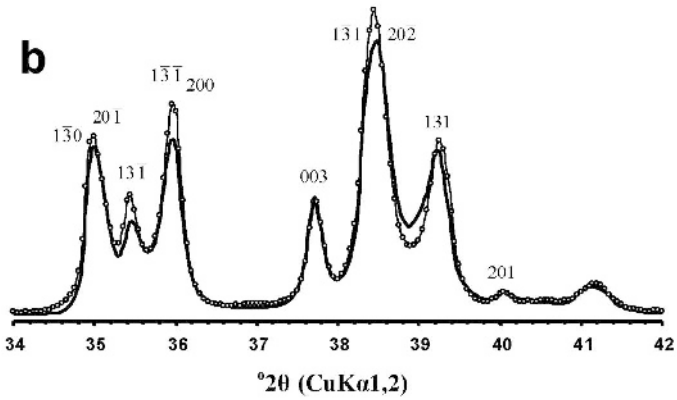

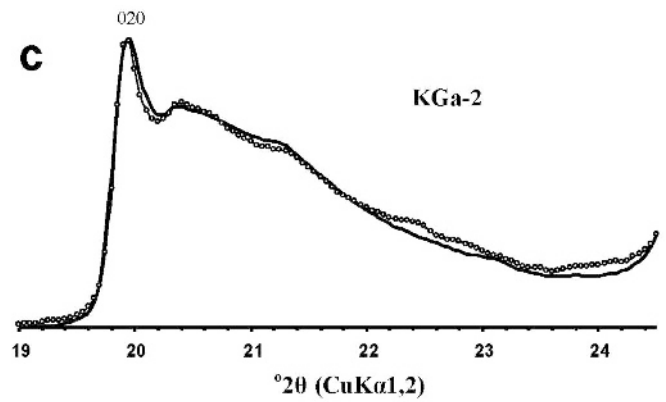

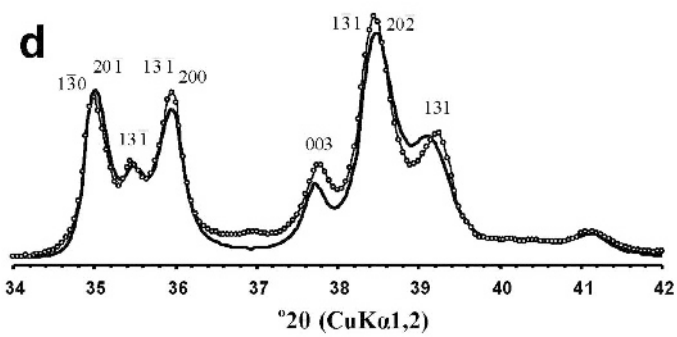

https://doi.org/10.1346/CCMN.2016.0640307 Published online by Cambridge University Press

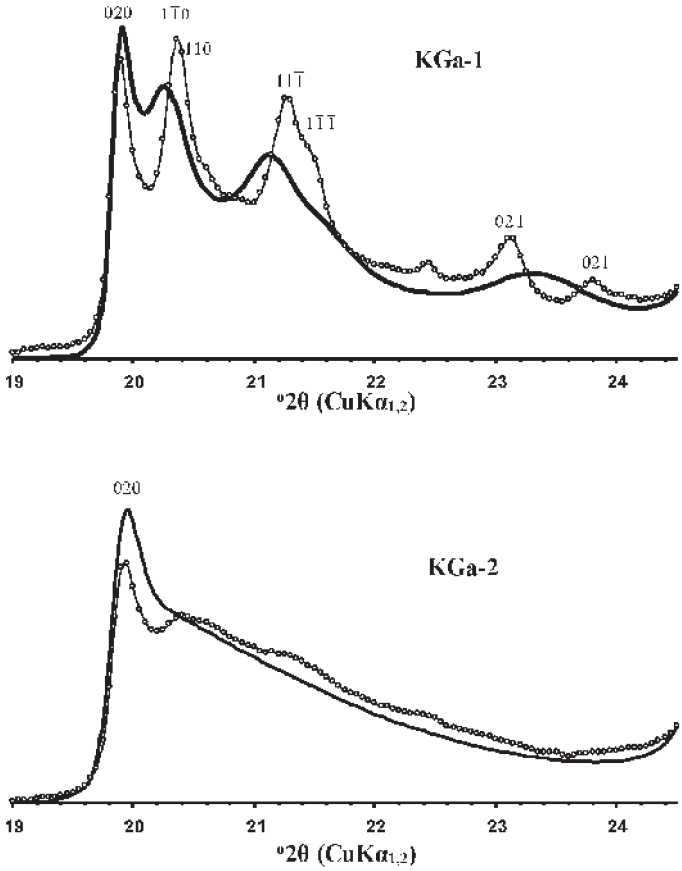

Figure 10. Parts of experimental KGa-1 and KGa-2 XRD patterns containing reflections in the 02*l*, 11*l* region compared with patterns calculated for a model in which the HOK and LOK components of both samples contain 10% layer displacements of $\mathbf{t}_1 - b/3$ instead of the $\mathbf{t}_1$ and $\mathbf{t}_2$ displacements.

other unusual defects that can provide a reasonably good fit with the experimental XRD pattern cannot be excluded. Variable parameters which have clear crystal-chemical meaning, however, are preferred to describe realistic structure models.

Stacking disorder by layer rotation and/or displacement of vacant octahedral sites. Application of HRTEM to the kaolinite sample of sedimentary origin previously studied by Johnston *et al*. (2008) showed that along with interstratification of left- and right-hand structural fragments, the studied kaolinite sample contains another type of stacking disorder related to either mutual layer rotation or to displacement of the octahedral vacancy site in the kaolinite layer (Kogure *et al*., 2010, Kogure, 2011). The geometrical analysis of these stacking faults carried out by Bookin *et al*. (1989) showed that the sequence of kaolinite layers containing stacking faults formed due to layer rotation or the octahedral vacancy displacements cannot be described in terms of the same lattice without mutual layer distortion. This distortion probably increases the energy of the formation of these stacking faults and decreases the occurrence probability.

Relationships between structural disorder recorded in a particle population and CSDs in the population.

According to definition, a CSD is formed by a set of strictly parallel layers providing coherent scattering of X-rays, neutrons, and electrons. Individual particles are usually an aggregate of CSDs which may have defect-free as well as similar or different defect structures. An individual particle, therefore, is characterized by statistically weighted structural disorder. Particles of a sample usually have a size distribution and with increasing size, the structural disorder of particles may either increase, decrease, or remain the same depending on the structural features of the CSDs that compose each particle-size fraction (Bish and Chipera, 1998).

To illustrate, let us consider the variation of the phase composition and structural features as a function of particle size for KGa-1 and KGa-2 as determined by Drits and Derkowski (2015). The KGa-2 sample has the same phase composition and structural disorder independent of the particle-size fraction. Particles of different sizes have the same proportion of the HOK and LOK phases and the same XRD characteristics.

https://doi.org/10.1346/CCMN.2016.0640307 Published online by Cambridge University Press

KGa-1 has a bimodal particle-size distribution with a coarser fraction of lower structural order albeit higher CSDs or crystallite thickness, whereas the finest size fraction has higher stacking order and is associated with thinner crystallites. Finally, the finer fractions of KGa-1 particles contain a higher proportion of the HOK phase compared with the bulk sample. Predicting the relationship between the structural and compositional features of each particle size fraction in advance is, therefore, difficult even if the phase composition and structural features of CSDs that compose a sample are known.

Reappraisal of kaolinite defect models suggested in the literature

Artioli et al. (1995) model. This model describes a structural disorder in natural kaolinites based on the stacking of B- and C-vacant layers and the enantiomorphs. Here the structure of each crystallite contains four layer displacement vectors $\mathbf{t}_1$, $\mathbf{t}_2$, $\mathbf{t}'_1$, and $\mathbf{t}'_2$ with occurrence probabilities derived from the probability recursive matrix. According to this model, a defect structure of well and poorly crystallized kaolinite with diffraction features similar to KGa-1 and KGa-2 can be described in terms of a single phase structural model; however, the incommensurability that should occur in BC and CB layer sub-sequences where comparable amounts of C layers and B layers coexist was not considered. The authors applied this approach to the kaolinite sample of hydrothermal origin named KAOSAR, which has an XRD pattern similar to the KGa-1 and KGa-2 standards. Even a visual observation of figure 9 in Artioli *et al*. (1995) demonstrates a strong disagreement between the experimental and modeled XRD patterns. Taking into account the crystal-chemical problems related to incorporating C- and B-vacant layers and the enantiomorphs, along with the poor calculated fit with the experimental data, this model can be rejected.

What is the highest probability of layer displacements $\mathbf{t}_0$ *that can exist in kaolinite structure?* In this study, special attention was paid to see the influence of $\mathbf{t}_0$ translation on the diffraction effects because of recent publications by White *et al*. (2013a,b). These authors showed that vibration dynamics of the crystal structure of natural kaolinite, KGa-1b, calculated using the density functional theory, agrees well with the experimental inelastic neutron scattering (INS) spectrum except for distinct discrepancies in the low frequency region (200–400 cm^{-1}). Analysis of possible types of stacking faults in the kaolinite structure, carried out by these authors, showed that the agreement between the calculated and observed low frequency regions are improved through the emergence of longer hydrogen bonds (O–H···O) that occur due to the formation of stacking faults from the layer displacement vector $\mathbf{t}_0$. The residual disagreement between the experimental and calculated spectra in the low frequency region was attributed to quantum tunneling of the inner surface H atoms associated with the hydrogen bonds (O–H···O). This effect should lead to a softening of the low frequency modes in the experimental spectrum compared to the calculated spectrum.

White *et al*. (2013a) concluded that the layer displacements by $\mathbf{t}_0$ are the dominant stacking fault in KGa-1b kaolinite because this defect resolved the discrepancy between experiment and theory for the H-atom dynamic in kaolinite. Because of the lack of direct evidence of layer displacements by $\mathbf{t}_0$ in the kaolinite structure, a set of calculations was carried out in this study to support or reject a $\mathbf{t}_0$ based model. In particular, XRD patterns for models of KGa-1b and KGa-2 samples in which the LOK phases contain different contents of these stacking faults were calculated. Even a model with 15% of the $\mathbf{t}_0$ layer displacements in the LOK phase of KGa-2 dramatically changed the positions and intensity distribution in both the 02*l*, 11*l* and 20*l*, 13*l* regions in the simulated XRD patterns compared with those in the experimental patterns (Figure 11a,b). Similar discrepancies were observed between the experimental XRD pattern and that calculated for a model in which the LOK phase of KGa-1 contains 20% of the $\mathbf{t}_0$ stacking faults (Figure 11c,d).

The positions of 02*l* and 11*l* reflections in the experimental XRD pattern of KGa-1b almost coincide with those of the HOK phase showing that this phase is almost defect free and has a structure close to that of the periodic 1*T*c kaolinite (Figures 3, 4). In contrast, the positions and intensity distribution of *hkl* reflections of the periodic structure formed by $\mathbf{t}_0$ layer displacements differed dramatically from those in the experimental XRD pattern (Figure 12). The obvious reason is that layer sequences whose formation is governed either by $\mathbf{t}_1$ or $\mathbf{t}_0$ layer displacements have principally different structures and, therefore, different positions and intensities of *hkl* reflections. Indeed, the direction of the $\mathbf{t}_0$ layer displacements coincides in projection on the *ab* plane with the long diagonal of the oblique kaolinite unit cell of the C-vacant layers. The degree of disagreement between the compared XRD patterns increases strongly when $\mathbf{t}_0$ layer displacements are introduced into the HOK structure (Figure 12). The layer sequence should, therefore, correspond to a monoclinic unit cell (Bailey, 1988). Indexing of *hkl* reflections in the XRD pattern calculated for a model in which layer displacements are governed only by $\mathbf{t}_0$ (Figure 12) allowed determination of a new set of unit cell parameters: a = 5.1805 Å, b = 8.9435 Å, c = 7.4069 Å, and β = 105.0°, which provide a good agreement between the observed and calculated d_{hkl} values.

Thus, the results obtained in the present paper show that the conclusion of White *et al*. (2013a,b) concerning the nature of the dominant type of stacking faults does not correspond to the actual structure of KGa-1b kaolinite. Therefore, the theoretical problem related to

https://doi.org/10.1346/CCMN.2016.0640307 Published online by Cambridge University Press

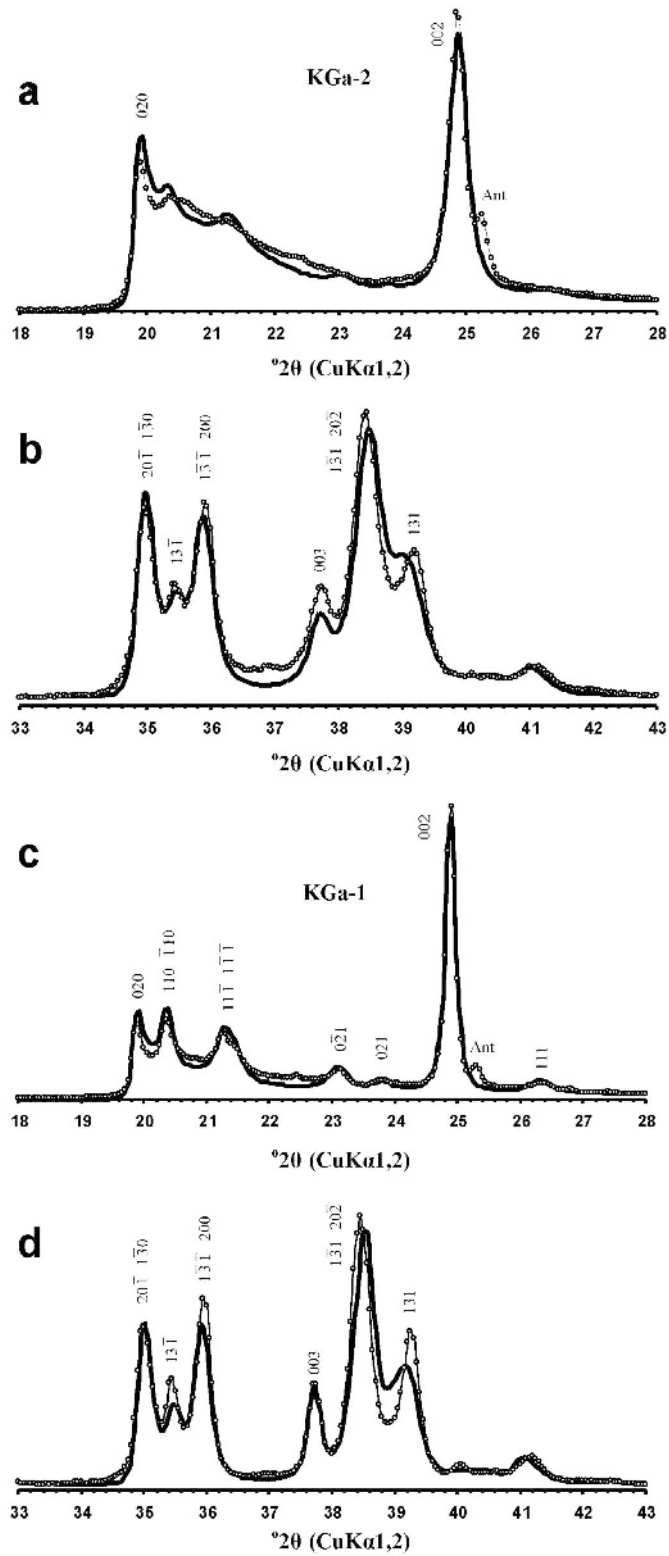

Figure 11. Comparison of the 02*l*, 11*l* (a) and 20*l*, 13*l* (b) regions in the experimental KGa-2 XRD patterns (dotted lines) with patterns obtained by optimal summation of calculated XRD patterns of the HOK and LOK phases (solid lines) in which the content of $\mathbf{t}_0$ stacking faults in the LOK phase was increased from 5 to 15%. Comparison of the 02*l*, 11*l* (c) and 20*l*, 13*l* (d) regions in the experimental KGa-1 XRD patterns (dotted lines) with patterns obtained by optimal summation of calculated XRD patterns of the HOK and LOK phases (solid lines) in which the content of $\mathbf{t}_0$ stacking faults in the LOK phase was increased from 5 to 20%.

https://doi.org/10.1346/CCMN.2016.0640307 Published online by Cambridge University Press

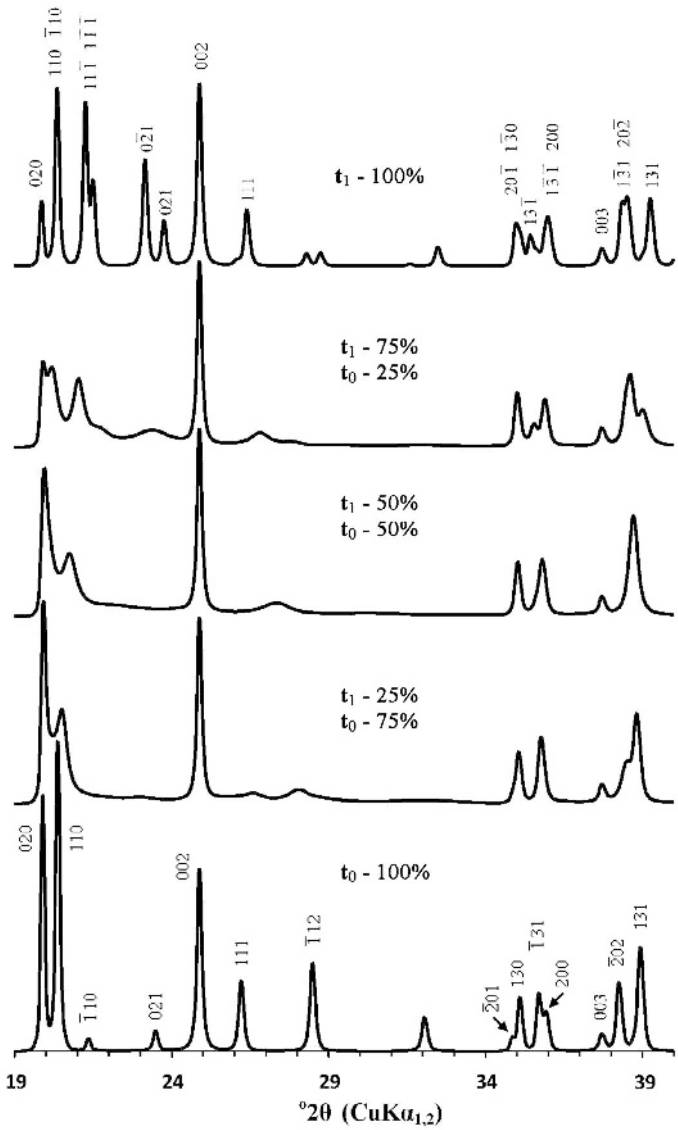

Figure 12. The evolution of positions and intensities of 02*l*, 11*l*, 20*l*, and 13*l* reflections in the XRD patterns calculated for models in which the contents of the interstratified $\mathbf{t}_0$ and $\mathbf{t}_1$ layers change from 0 to 100%.

interpretation of the low frequency modes in the experimental INS spectra of kaolinite samples requires further investigation.

Why knowledge of the actual kaolinite structures may be useful for interpretation of experimental data? As was mentioned, Paris (2014) discovered that two aluminum sites in the ^{27}Al MAS NMR spectrum of KGa-1b have different spectral parameters. According to the author, although the spectrum decomposition was very accurate, the experimental NMR parameter values must be justified independently, which was the actual problem. The choice of the KGa-1b sample was based on a firm belief that the sample contains a low defect content. Therefore, to confirm the validity of the spectral parameters obtained for two aluminum sites, the kaolinite structure with 3D periodicity was chosen for first-principle calculations of the NMR parameters. As was shown in the present study, the KGa-1b sample has a 28.4% defect-free phase; where 71.6% of the phase has a comparable amount of right- and left-hand kaolinite structural fragments that are interstratified at random. The application of first-principle calculations of the NMR parameters from the periodic kaolinite structure cannot, therefore, be considered as independent evidence of the validity of the experimental spectroscopic data obtained from the sample with a high content of stacking faults.

https://doi.org/10.1346/CCMN.2016.0640307 Published online by Cambridge University Press

ACKNOWLEDGMENTS

The work was supported by the budget project #0135-2014-0032, Geological Institute RAS.

REFERENCES

Artioli, G., Bellotto, M., Gualtieri, A., and Pavese, A. (1995) Nature of structural disorder in natural kaolinites: a new model based on computer simulation of powder diffraction data and electrostatic energy calculation. *Clays and Clay Minerals*, **43**, 438–445.

Bachmaf, S. and Merkel, B.J. (2011) Sorption of uranium (VI) at the clay mineral water interface. *Environmental Earth Sciences*, **63**, 925–934.

Bailey, S.W. (1963) Polymorphism of the kaolinite minerals. *American Mineralogist*, **48**, 1196–1209.

Bailey, S.W. (1988) Polytypism of 1:1 layer silicates. Pp. 9–27 in: *Hydrous Phyllosilicates (Exclusive of Micas)* (S.W. Bailey, editor). Reviews in Mineralogy, **19**. Mineralogical Society of America, Chantilly, Virginia, USA.

Balan, E., Saitta, A.M., Mauri, F., and Calas, G. (2001) First-principles modeling of the infrared spectrum of kaolinite. *American Mineralogist*, **86**, 1321–1330.

Balan, E., Delattre, S., Guillaumet, M., and Salje, E.K.H. (2010) Low-temperature infrared spectroscopic study of OH-stretching modes in kaolinite and dickite. *American Mineralogist*, **95**, 1257–1266.

Bellotto, M., Gualtieri, A., Artioli, G., and Clark, S.M. (1995) Kinetic study of the kaolinite-mullite reaction sequence. Part I: Kaolinite dehydroxylation. *Physics and Chemistry of Minerals*, **22**, 207–214.

Bish, D.L. and Chipera, S.J. (1998) Variation of kaolinite defect structure with particle size. *Proceedings of the 35th Annual Clay Minerals Society Meeting, Cleveland, Ohio*, p. 90.

Bish, D.L. and von Dreele, R.B. (1989) Rietveld refinement of non-hydrogen atomic positions in kaolinite. *Clays and Clay Minerals*, **37**, 289–296.

Brindley, G.W. (1980) Order-disorder in clay mineral structure. Pp. 125–196 in: *Crystal Structure of Clay Minerals and their X-ray identification* (G.W. Brindley and G. Brown, editors). Monograph **5**, Mineralogical Society of Great Britain and Ireland, London.

Brindley, G.W. and Nakahira M. (1958) The kaolinite-mullite reaction. Series: II Metakaolinite. *Journal of the American Ceramic Society*, **42**, 314–318.

Brindley, G.W. and Robinson, K. (1946) The structure of kaolinite. *Mineralogical Magazine*, **27**, 242–253.

Brindley, G.W., Kao, C.C., Harrison, J.L., Lipsicas, M., and Raythatha, R. (1986) Relation between structural disorder and other characteristics of kaolinites and dickites. *Clays and Clay Minerals*, **34**, 239–249.

Bookin, A.S., Drits, V.A., Plançon, A., and Tchoubar, C. (1989) Stacking faults in kaolin-group minerals in the light of real structural features. *Clays and Clay Minerals*, **37**, 297–307.

Chipera, S.J. and Bish, D.L. (2001) Baseline studies of The Clay Mineral Society Source Clays: Powder X-ray diffraction analyses. *Clays and Clay Minerals*, **49**, 398–409.

Drits, V.A. and Derkowski, A. (2015) Kinetic behavior of partially dehydroxylated kaolinite. *American Mineralogist*, **100**, 883–896.

Drits, V.A. and Tchoubar, C. (1990) *X-ray Diffraction by Disordered Lamellar Structures*. Springer-Verlag. Berlin, Heidelberg. 371 pp.

Drits, V.A., Sakharov, B.A., Lindgreen, H., and Salyn, A. (1997a) Sequential structural transformation of illite-smectite-vermiculite during diagenesis of Upper Jurassic shales from North Sea and Denmark. *Clay Minerals*, **32**, 351-372

Drits, V.A., Środoń, J., and Eberl, D.D. (1997b) XRD measurements of mean crystallite thickness of illite and illite/smectite: Reappraisal of the Kubler index and the Scherrer equation. *Clays and Clay Minerals*, **45**, 461–475.

Drits, V.A., Kameneva, M.Y., Sakharov, B.A., Dainyak, L.G., Tsipursky, S.I., Smoliar-Zviagina, B.B., Bookin, A.S., and Salyn, A.L. (1993) The actual structure of glauconites and related mica-like minerals. *Nauka*, Novosibirsk.180 pp. (in Russian).

Drits, V.A., Sakharov, B.A., Dainyak, L.G., Salyn, A.L., and Lindgreen, H. (2002a) Structural and chemical heterogeneity of illite-smectites from Upper Jurassic mudstones of East Greenland related to volcanic and weathered parent rocks. *American Mineralogist*, **87**, 1590–1607.

Drits, V.A., Lindgreen, H., Sakharov, B.A., Jakobsen, H.J., Salyn, A.L., and Dainyak, L.G. (2002b) Tobelitization of smectite during oil generation in oil-source shales. Application to North Sea illite-tobelite-smectite-vermiculite. *Clays and Clay Minerals*, **50**, 82–98.

Drits, V.A., Derkowski, A., and McCarty, D.K. (2011a) New insight into the structural transformation of partially dehydroxylated pyrophyllite. *American Mineralogist*, **96**, 153–171.

Drits, V.A., Derkowski, A., and McCarty, D.K. (2011b) Kinetics of thermal transformation of partially dehydroxylated pyrophyllite. *American Mineralogist*, **96**, 1504–1069.

Ferrage, E., Lanson, B., Sakharov, B.A., Geoffroy, N., Jacquot, E., and Drits, V.A. (2007) Investigation of dioctahedral smectite hydration properties by modeling of X-ray diffraction profiles: influence of layer charge and charge location. *American Mineralogist*, **92**, 1731–1743.

Franco, F., Pérez-Maqueda, L.A., and Perez-Rodriguez, J. (2004) The effect of ultrasound on the particle size and structural disorder of a well ordered kaolinite. *Journal of Colloid and Interface Science*, **274**, 107–117.

Frost, R.L. and Vassallo, A.M. (1996) The dihydroxylation of the kaolinite clay minerals using infrared emission spectroscopy. *Clays and Clay Minerals*, **44**, 635–651.

Giese, R.F. (1982) Theoretical studies of the kaolinite minerals: Electrostatic calculations. *Bulletin de Minéralogie*, **105**, 417–424.

Hinckley, D.N. (1963) Variability in "crystallinity" values among the kaolin deposits of the coastal plain of Georgia and South Carolina. *Clays and Clay Minerals*, **11**, 229–235.

Johnston, C.T., Agnew, S.F., and Bish, D.L. (1990) Polarized single-crystal Fourier-transform infrared microscopy of Ouray dickite and Keokuk kaolinite. *Clays and Clay Minerals*, **38**, 573–583.

Johnston, C.T., Kogel, J.E., Bish, D.L., Kogure, T., and Murray, H.H. (2008) Low-temperature FTIR study of kaolin-group minerals. *Clays and Clay Minerals*, **56**, 470–485.

Kogure, T. (2011) Stacking disorder in kaolinite revealed by HRTEM: a review. *Clay Science*, **15**, 3–11.

Kogure, T. and Inoue, A. (2005) Determination of defect structures in kaolin minerals by high-resolution transmission electron microscopy (HRTEM). *American Mineralogist*, **90**, 85–89.

Kogure, T., Johnston, C.T., Kogel, J.E., and Bish, D. (2010) Stacking disorder in a sedimentary kaolinite. *Clays and Clay Minerals*, **58**, 63–72.

Lanson, B., Sakharov, B.A., Claret, F., and Drits, V.A. (2009) Diagenetic smectite-to-illite transition in clay-rich sediments: a reappraisal of X-ray diffraction results using the multi-specimen method. *American Journal of Science*, **309**, 476–516.

Lindgreen, H., Drits, V.A., Sakharov, B.A., Jakobsen, H.J.,

Salyn, A.L., Dainyak, L.G., and Krøyer, H. (2002) The structure and diagenetic transformation of illite-smectite and chlorite-smectite from North Sea Cretaceous-Tertiary chalk. *Clay Minerals*, **37**, 429–450.

Madejová, J. and Komadel, P. (2001) Baseline studies of The Clay Mineral Society Source Clays: Infrared methods. *Clays and Clay Minerals*, **49**, 410–432.

McCarty, D.K., Sakharov, B.A., and Drits, V.A. (2009) New insights into smectite illitization: A zoned K-bentonite revisited. *American Mineralogist*, **94**, 1653–1671.

Mermut, A.R. and Cano, A.F. (2001) Baseline studies of The Clay Mineral Society Source Clays: Chemical analyses of major elements. *Clays and Clay Minerals*, **49**, 381–386.

Moll, W.F., Jr. (2001) Baseline studies of The Clay Mineral Society Source Clays: Geological origin. *Clays and Clay Minerals*, **49**, 374–380.

Murray, H.H. (1954) Structural variation of some kaolinites in relation to dehydroxylated halloysite. *American Mineralogist*, **39**, 97–108.

Newnham, R.E. (1961) A refinement of the dickite structure and some remarks on polymorphism in kaolinite minerals. *Mineralogical Magazine*, **32**, 683–704.

Paris, M. (2014) The two aluminum sites in the ^{27}Al MAS NMR spectrum of kaolinite: Accurate determination of isotopic chemical shifts and quadrupolar interaction parameters. *American Mineralogist*, **99**, 393–400.

Plançon, A. and Tchoubar, C. (1977) Determination of structural defects in phyllosilicates by X-ray powder diffraction- II. Nature and proportion of defects in natural kaolinites. *Clays and Clay Minerals*, **25**, 436–450.

Plançon, A. and Zakharie, C. (1990) An expert system for the structural characterization of kaolinites. *Clay Minerals*, 25, 249–260.

Plançon, A., Giese, R.F., Snyder, R., Drits, V.A., and Bookin, A.S. (1989) Stacking faults in the kaolin-group mineral-defect structures of kaolinite. *Clays and Clay Minerals*, **37**, 203–210.

Pruett, R.J. and Webb, H.L. (1993) Sampling and analysis of KGa-1b well crystallized kaolin source clay. *Clays and Clay Minerals*, **41**, 514–519.

Reynolds, Jr., R.C. (1986) The Lorentz-polarization factor and preferred orientation in oriented clay aggregates. *Clays and Clay Minerals*, **34**, 359–367.

Sakharov, B.A., Lindgreen, H., Salyn, A.L., and Drits V.A. (1999) Determination of illite-smectite structures using multispecimen X-ray diffraction profile fitting. *Clays and Clay Minerals*, **47**, 555–566.

Sakharov, B.A., Plançon, A., Lanson, B., and Drits, V.A. (2004) Influence of the outer surface layers of crystals on the X-ray diffraction intensity of basal reflections. *Clays and Clay Minerals*, **52**, 680–692.

Schroth, B.K. and Sposito, G. (1997) Surface charge properties of kaolinite. *Clays and Clay Minerals*, **45**, 85–91.

Sperinck, S., Raiteri, P., Marks, N., and Wright, K. (2011) Dehydroxylation of kaolinite to metakaolin – a molecular dynamics study. *Journal of Materials Chemistry*, **21**, 2118–2125.

Suitch, P.R. and Young, R.A. (1983) Atom position in highly ordered kaolinite. *Clays and Clay Minerals*, **31**, 357–366.

Sutheimer, S., Maurice, P.A., and Zhou, Q. (1999) Dissolution of well and poorly crystallized kaolinites: Al speciation and effects of surface characteristics. *American Mineralogist*, **84**, 620–628.

Ufer, K., Kleeberg, R., and Monecke, T. (2015) Quantification of stacking disordered Si-Al layer silicates by the Rietveld method: application to exploration for high-sulphidation epithermal gold deposits. *Powder Diffraction*, **30**, suppl 1. 111–118.

Van Olphen, H. and Fripiat, J.J. (1979) *Data Handbook for Clay Minerals and Other Non-metallic Minerals.* Pergamon Press, Oxford, UK, 346 pp.

White, C.E., Provis, J.L., Riley, D.P., Kearley, G.J., and van Deventer, J.S.J. (2009) What is the structure of kaolinite? Reconciling theory and experiment. *Journal Physical Chemistry*, **113**, 6756–6765.

White, C.E., Provis, J.L., Proffen, T., Riley, D.P., and van Deventer, J.S.J. (2010) Density functional modeling of the local structure of kaolinite subjected to thermal dehydroxylation. *Journal of Physical Chemistry A*, **114**, 4988–4996.

White, C.E., Kearley, G.J., Provis, J.L., and Riley, D.P. (2013a) Inelastic neutron scattering analysis of the thermal decomposition of kaolinite to metakaolin. *Chemical Physics*, **427**, 82–86.

White, C.E., Kearley, G.J., Provis, J.L., and Riley, D.P. (2013b) Structure of kaolinite and influence of stacking faults: reconciling theory and experiment using inelastic neutron scattering analysis. *The Journal of Chemical Physics*, **138**, 194501–194507.

Wu, W. (2001) Baseline studies of The Clay Mineral Society Source Clays: Colloid and surface phenomena. *Clays and Clay Minerals*, **49**, 446–452.

(*Received 27 January 2016; revised 10 June 2016; Ms. 1085; AE: E. Ferrage*)